Future Evolution of the Intergalactic Medium in a Universe Dominated by a Cosmological Constant

Kentaro Nagamine [1], Abraham Loeb [2]

Harvard-Smithsonian Center for Astrophysics, 60 Garden Street, MS 51, Cambridge, MA 02138

Abstract

We simulate the evolution of the intergalactic medium (IGM) in a universe dominated by a cosmological constant. We find that within a few Hubble times from the present epoch, the baryons will have two primary phases: one phase composed of low-density, low-temperature, diffuse, ionized gas which cools rapidly with cosmic time due to adiabatic exponential expansion, and a second phase of high-density, high-temperature gas in virialized dark matter halos which cools much more slowly by atomic processes. The mass fraction of gas in halos converges to $\sim 40\%$ at late times, about twice its calculated value at the present epoch. We find that in a few Hubble times, the large scale filaments in the present-day IGM will rarefy and fade away into the low-temperature IGM, and only islands of virialized gas will maintain their physical structure. We do not find evidence for fragmentation of the diffuse IGM at later times. More than 99% of the gas mass will maintain a steady ionization fraction above 80% within a few Hubble times. The diffuse IGM will get extremely cold and dilute but remain highly ionized, as its recombination time will dramatically exceed the age of the universe.

Key words: cosmology: theory, cosmology: large-scale structures, methods: numerical

1 Introduction

Independent data sets, involving the temperature anisotropies of the cosmic microwave background (de Bernardis et al., 2000; Hanany et al., 2000; Spergel

[1] E-mail: knagamin@cfa.harvard.edu
[2] E-mail: aloeb@cfa.harvard.edu

et al., 2003), the luminosity distances of Type Ia supernovae (Garnavich et al., 1998; Riess et al., 1998; Perlmutter et al., 1999; Hanany et al., 2000), the large-scale distribution of galaxies (Peacock et al., 2001; Verde et al., 2002), and cluster abundances (Eke et al., 1998; Bahcall & Bode, 2003), appear to be all consistent with a single set of cosmological parameters. In the concordance Λ–Cold Dark Matter (ΛCDM) model, the universe is flat and its expansion rate is currently accelerating; the cosmic mass density is dominated ($\sim 70\%$) by the vacuum (the so-called cosmological constant or "dark energy") with the remaining density mostly in the form of cold dark matter ($\sim 26\%$) and baryons ($\sim 4\%$).

Given the emergence of a standard model in cosmology with a specific set of parameters, it is of much interest to follow the immediate consequence of these parameters in terms of the near future evolution of the ΛCDM universe. While several recent studies considered the qualitative implications of the accelerating universe by analytic means (Adams & Laughlin, 1997; Krauss & Starkman, 2000; Chiueh & He, 2002; Gudmundsson & Björnsson, 2002; Loeb, 2002), it is clear that further quantitative insight can be gained only through direct numerical simulations. In Nagamine & Loeb (2003, hereafter Paper I), we simulated the evolution of nearby large-scale structure using a constrained realization of the Local Universe with only dark matter particles. We have found that structure will freeze within two Hubble times from the present epoch, and that the dark matter halo mass function will not evolve subsequently. Busha et al. (2003) further studied the generic evolution of the density profile around dark matter halos embedded in an accelerating universe.

In this paper we extend previous numerical work and study the evolution of the baryonic component of the universe using a hydrodynamic cosmological simulation. In Section 2 we describe the simulation. Images of the simulated gas mass distribution and gas temperature distribution are presented in Section 3. We describe the global evolution of gas temperature and overdensity in Section 5, and provide a more quantitative analysis based on the distribution functions of these quantities in Section 6 and 7. The ionization fraction of cosmic gas is analyzed in Section 8. Finally, we summarize our main conclusions in Section 9.

2 Simulation

We carried out a hydrodynamic simulation with the concordance cosmological parameters ($\Omega_{M,0}$, $\Omega_{\Lambda,0}$, Ω_b, h, σ_8, n)=(0.3, 0.7, 0.04, 0.7, 0.9, 1.0) from a redshift $z = 99$ (i.e. a scale factor $a = (1+z)^{-1} = 0.01$) through the present time ($z = 0$, $a = 1$), and up to 6 Hubble times into the future ($a = 166$; ~ 84 billion years from today). Because the present Hubble time $t_{\rm H} \equiv 1/H_0 = 14$

Gyr is very close to the current age of the Universe $t_0 = 13.5$ Gyr in the adopted cosmology, the epoch of $a = 166$ roughly corresponds to $t = t_0 + 6t_{\rm H} \approx 7t_{\rm H}$ from the Big Bang ($t = 0$), where a subscript zero denotes present-day values.

We use the updated version of the parallel tree Smoothed Particle Hydrodynamics (SPH) code GADGET [1] (Springel et al., 2001). The comoving box size of our simulation is $50h^{-1}$ Mpc, and the particle number is 64^3 for the gas and 64^3 for the dark matter, with corresponding particle masses $m_{\rm DM} = 3.4 \times 10^{10} h^{-1} M_\odot$ and $m_{\rm gas} = 5.3 \times 10^9 h^{-1} M_\odot$ (so that a group of ~ 50 particles has a total mass comparable to that of the Milky Way galaxy). We adopt the 'entropy-conserving' formulation of SPH as described by Springel & Hernquist (2002). The simulation includes a standard treatment of the radiative cooling and heating of Katz et al. (1996) assuming that the gas is optically thin and in ionization equilibrium (see Section 8 for the discussion on the validity of this assumption at late times). The abundance of different ionic species, including H^0, He^0, H^+, He^+, and He^{++}, is computed by solving the network of equilibrium equations self-consistently with a uniform ultra-violet (UV) background radiation of a modified Haardt & Madau (1996) spectrum and with complete reionization at $z \sim 6$ (Davé et al., 1999; Becker et al., 2001). The UV background (or, equivalently, the photoionization rate Γ of the IGM) is linearly extrapolated beyond the present epoch, after which it quickly approaches zero. We have tested the validity of this assumption by carrying out another simulation with a maximum UV background field, where the value of the photoionization rate was set equal to the $z = 0$ value and remained constant afterwards. Even for this maximum UV background field, the future thermal evolution of the IGM remained similar. The exact behavior of the UV background field after $z = 0$ is unimportant because the photoionization time-scale is rapidly increasing to values much longer than the Hubble time. This follows from the fact that the cosmic volume element (by which the ionizing photons are diluted) grows as $\propto a^3$ and a grows exponentially with cosmic time, i.e. $a \propto \exp\{\sqrt{\Omega_{\Lambda,0}} H_0 t\}$ at $t \gg t_0$. The evolution of the neutral hydrogen mass density in a similar simulation run was discussed by Nagamine et al. (2003a).

Feedback from star formation and supernovae is formulated as in Springel & Hernquist (2003a,b); the underlying assumptions are also reviewed in Nagamine et al. (2003b). However, the details of the adopted star formation model should not be very important for the results presented here since the heating of the gas on large scales is dominated by the gravitationally-induced shocks. Although the numerical resolution of our simulation is not adequate for following the detailed star formation history of the Universe (see Springel & Hernquist, 2003b), it does capture well the large-scale properties of baryons in the IGM

[1] http://www.MPA-Garching.MPG.DE/gadget/

which are the focus of this work. Future simulation runs with a higher resolution and an improved model of star formation and supernova feedback could address more complicate issues, such as the distribution of metals in the IGM.

Our simulation was performed at the Center for Parallel Astrophysical Computing [2] at Harvard-Smithsonian Center for Astrophysics.

3 Images

Figure 1 shows the projected distribution of mass-weighted temperature (left column) and the mass surface density (right column) of the gas as functions of cosmic time in a slice with a comoving thickness of $10h^{-1}$ Mpc and a comoving width of $50h^{-1}$ Mpc on a side.

As shown in Paper I, the evolution of large-scale structure in the dark matter distribution freezes within two Hubble times from the present epoch. Similarly, the right column of Figure 1 indicates that the gas distribution does not evolve either at late times. The only noticeable change in comoving coordinates relative to the present epoch is that the filaments thin out as their mass is drained into X-ray clusters. The two visible X-ray clusters (one at the top middle and the other at the bottom middle of this simulation) are still connected by a low-temperature filament of gas and dark matter even at $t = t_0 + 6t_{\rm H}$. In physical coordinates, these filaments rarefy considerably as the universe expands exponentially with cosmic time.

Due to the adiabatic expansion of the IGM, the temperature distribution of the cosmic gas evolves dramatically with time. At $t = t_0$, the high-temperature clusters (with $T > 10^7$ K, indicated by yellow) are connected by filaments with a somewhat lower temperature ($10^5 < T < 10^7$ K, indicated by red). As time progresses, the red filaments cool down ($T < 10^5$ K in green), get thinner, and eventually disappear into the dark background. Consequently, virialized dark matter halos with gas temperature $T \geq 10^4$ K are left as 'island universes' embedded within the low-temperature IGM.

In principle, it is possible for the IGM to fragment into baryonic objects (which do not necessarily overlap with dark matter halos) due to its rapid adiabatic cooling. We have tested for this possibility by applying the HOP grouping algorithm (Eisenstein & Hut, 1998) to the gas particles in the simulation, but found no evidence for such fragmentation. We caution, however, that our numerical resolution is not adequate for probing fragmentation below the mass-scale of $M_{gas} \sim 5 \times 10^{11} h^{-1} M_\odot$.

[2] http://cfa-www.harvard.edu/cpac/

4 Growth Factor

In order to demonstrate the freezing of the structure formation in the future from a different perspective, we examine the evolution of the growth factor of linear density fluctuations in a ΛCDM universe. Figure 2 shows the growth factor (Heath, 1977; Carroll, Press, & Turner, 1992) as a function of the logarithm of the scale factor, a,

$$D(a) \propto \frac{1}{a}\frac{da}{d\tau}\int_0^a \left(\frac{da'}{d\tau}\right)^{-3} da', \tag{1}$$

where

$$\left(\frac{da}{d\tau}\right)^2 = 1 + \Omega_{M,0}\left(\frac{1}{a} - 1\right) + \Omega_{\Lambda,0}(a^2 - 1), \tag{2}$$

and $\tau = H_0 t$. The curve is normalized to unity at $a = 1$. It clearly demonstrates that the growth of structure ceases at about two Hubble times from the present time in a Universe which is dominated by a cosmological constant, consistently with the results of Paper I. This saturation is caused by the exponential expansion of $a(t)$ as driven by the cosmological constant.

5 Temperature – Density Diagram

Next we project the global evolution of the gas properties on the temperature–gas density (T–ρ) plane. In Figure 3 we show the mass-weighted distribution of baryons on the temperature – gas overdensity plane as a function of cosmic time. The time and corresponding scale factor values are indicated in each panel, and the plotted contours are equally spaced in six logarithmic intervals between the minimum and maximum values on the plane.

The top left panel shows the familiar geometry of the gas distribution at the present time; the solid line divides the gas into 3 different categories following the criteria of Davé et al. (2001). As shown later, the dividing line of $\rho/\langle\rho\rangle \equiv (1+\delta) = 10^3$ (where $\langle\rho\rangle$ is the mean density) has a special meaning in terms of the future evolution of the IGM as well. The bottom left region of the diagram corresponds to the diffuse IGM which has a low density and a low temperature. Most of the gas mass in this region lies on the tight nearly-adiabatic power-law relation, which can be described by analytic means (Hui & Gnedin, 1997). A plume-shaped region of shock-heated gas extends above the horizontal solid line at $T = 10^5$ K. The gas with temperatures $10^5 < T < 10^7$ K is the so

called *warm-hot intergalactic medium* (WHIM; Cen & Ostriker, 1999), and the dense gas with $T > 10^8$ K is the *hot* gas in clusters of galaxies. In the current study, the distinction between the *warm-hot* and *hot* gas is not particularly important, and so we simply refer to them both as *hot gas*. Finally, the bottom right portion of the diagram is occupied by condensed gas that has cooled radiatively inside dark matter halos.

Within two Hubble times into the future ($t = t_0 + 2t_{\rm H}$), the innermost contour line splits into two islands, one for the low-density diffuse IGM and the other for the gas in virialized dark matter halos. The overdensity of gas in dense regions increases with time because the physical density there remains nearly fixed while the background density rarefies rapidly due to its Hubble expansion.

The T–ρ diagram is stretched into a more elongated shape in the distant future. This elongation of the contour can be understood by considering the gas in clusters of galaxies that have $T = 10^{7.5}$ K and overdensity of 200 at $z = 0$. The Bremsstrahlung (which dominates the cooling rate at this temperature) cooling time of such gas is much longer than the current Hubble time:

$$t_{cool} \sim \frac{2 \cdot \frac{3}{2} kT}{\epsilon_B} \sim 10^2 \left(\frac{200}{\rho / \langle \rho \rangle_0} \right) \left(\frac{T}{10^{7.5}\ \mathrm{K}} \right)^{1/2} t_{\rm H}, \tag{3}$$

where $\epsilon_B \propto T^{0.5} \rho$ is the Bremsstrahlung cooling rate per electron at a temperature T and density ρ of the cluster gas. The factor of 2 in the numerator accounts for the thermal energy of the protons in addition to that of the cooling electrons. Because of this long cooling time, such gas in the outskirts of clusters of galaxies will remain hot in the distant future.

The contour peak at $T \sim 10^6$ K and $\log(\rho / \langle \rho \rangle) > 3.0$ corresponds to gas inside galaxies and groups of galaxies. For this gas, the significance of metal line cooling increases with time as the gas gets enriched with supernova ejecta, and the cooling time of the enriched gas is already shorter than the Hubble time at present. Since our simulation does not include metal cooling and star formation is not treated accurately due to lack of numerical resolution, we cannot rule out the possibility that the peak at $T \sim 10^6$ K disappears at late times.

After six Hubble times ($t = t_0 + 6t_{\rm H}$), the flat bottom of the contour plot reaches the temperature floor of $T = 5$ K, which is set by hand in the simulation and is not physical. The virialized gas maintains a temperature above $T = 10^4$ K because its cooling curve drops sharply below this temperature. The vertical solid line indicates the dividing overdensity of 10^3. The horizontal solid line at $T = 10^{3.2}$K will be discussed later.

6 Distribution & Evolution of Gas Overdensity

To describe the evolution of the IGM more quantitatively, we show in Figure 4 the mass-weighted distribution function of the cosmic gas as a function of its density contrast $df_M/d\log(\rho/\langle\rho\rangle)$ [panel (a)], and the cumulative mass fraction of gas with overdensity larger than a specific value $f_M(>\rho/\langle\rho\rangle)$ [panel (b)]. Hereafter, we denote the gas mass fraction in general by f_M.

Panel (a) indicates that the gas distribution becomes bimodal as time progresses; the bottom of the valley that separates the gas into two islands is located near a density contrast $\rho/\langle\rho\rangle \equiv 1+\delta = 10^3$ at $t = t_0 + 6t_{\rm H}$, as indicated by the vertical dotted line. This makes $1+\delta = 10^3$ a natural choice for the borderline separating the gas into its two phases: the diffuse IGM and the phase which remains bound in virialized dark matter halos (as marked by the solid lines in Figure 3).

Panel (b) shows that more gas shifts toward higher overdensities as it falls into the potential wells of dark matter halos at late times. This is partially because the physical density in virialized halos remains nearly the same while the background density rarefies rapidly due to the exponential expansion of the universe. From this panel, we derive the gas mass fraction that is in the region above some overdensity value, as indicated by the dashed lines. We find that the gas mass fraction with $1+\delta > 10^3$ is 10% (40%) at $t = t_0$ ($t = t_0 + 6t_{\rm H}$). The gas mass fraction with $1+\delta > 200$ is 22% (43%) at $t = t_0$ ($t = t_0 + 6t_{\rm H}$). Finally, the fraction with $1+\delta > 17.6$ is 47% (58%) at $t = t_0$ ($t = t_0 + 6t_{\rm H}$). These results are summarized in Figure 5, which shows the gas mass fraction $f_M(> 1+\delta_{\rm th})$ with density contrast higher than $1+\delta_{th} = \rho/\langle\rho\rangle = 17.6$ (solid), 200 (short-dashed), and 1000 (long-dashed line), as a function of cosmic time from the present epoch in units of the current Hubble time. This figure shows the convergence of the amount of gas that is trapped inside virialized dark matter halos in two Hubble times from the present time. The gas mass fractions with $1+\delta > 200$ and > 1000 both converge to $\sim 40\%$ at $t = t_0 + 6t_{\rm H}$. At the lower threshold overdensity of $1+\delta = 17.6$, the mass fraction increases to 58%. The threshold value of 17.6 was derived in Paper I as the critical overdensity above which mass remains bound to virialized objects at late times.

7 Distribution & Evolution of Gas Temperature

Figure 6 shows the mass-weighted distribution function of gas as a function of the logarithm of the temperature $df_M/d\log T$ [panel (a)], and the cumulative mass fraction of gas $f_M(>\log T)$ with a temperature larger than a certain

value [panel (b)].

Panel (a) shows that the minimum IGM temperature decreases as a function of time due to the expansion of the Universe, while the maximum temperature stays constant at $T = 10^8$ K due to the lack of growth in the potential well depth of dark matter halos. The artificial cutoff at the temperature floor of $T = 5$ K is set by hand in the simulation.

Panel (b) implies that the mass fraction of gas with $T > 10^5$ K is roughly 60% at $t = t_0$, and that this fraction decreases to 20% at $t = t_0 + 6t_{\rm H}$. The mass fraction of gas with $T > 10^{3.2}$ K is 40% at $t = t_0 + 6t_{\rm H}$ (corresponding to the mass fraction above $1 + \delta = 10^3$ in Figure 4).

Figure 7 shows the evolution of the maximum temperature for gas with a fixed gas mass fraction of 40% in lower density regions as a function of the logarithm of the scale factor. This quantity measures the evolution of the temperature at $f_M(\log T) = 0.6$ in panel (b) of Figure 6 because Figure 6 was a cumulative plot. Figure 7 indicates that the temperature of the diffuse IGM cools down roughly according to the adiabatic expansion law, $T \propto a^{-2}$, as illustrated by the dashed line. We confirmed that the result doesn't change very much even in the 'max-UV field' run which we described in Section 2.

Figure 8 shows the mean (mass-weighted) temperature of all the gas in the Universe, $\langle T \rangle$, as a function of the scale factor, $a = (1 + z)^{-1}$. The upper horizontal axis indicates the corresponding redshift, z. It can be seen that the beginning (redshifts $z > 20$) of the thermal history of the diffuse IGM are dominated by the adiabatic cooling. This is also true for the end of the thermal history of the diffuse IGM as we already showed in Figure 6. In between these two cooling phases, there is an epoch of structure formation during which the IGM is heated through large-scale shocks or the radiation emitted by stars and quasars. The value of $\langle T \rangle$ at late times is dominated by the gas trapped in virialized dark matter halos which will cool only slowly with cosmic time. Overall, we find that $\langle T \rangle$ will peak at a value of $\sim 2 \times 10^6$ K at $a \sim 2.5$, only one Hubble time (~ 14 billion years) from the present epoch. The appearance of the peak value of $\langle T \rangle$ in the relatively near future simply reflects the lack of subsequent growth in the mass function of virialized halos.

8 Ionization Fraction

Finally, we consider the ionization fraction of the cosmic gas, which we define as

$$F_{\rm ion} = \frac{n_e}{n_e + n_n}, \tag{4}$$

where n_e is the electron number density, and n_n is the total number density of neutral atoms. Since our simulation includes only the ionization of hydrogen and helium, $n_n = n_{\rm HI} + n_{\rm HeI}$. With this definition, $F_{\rm ion} \to 1$ for a fully ionized gas and $F_{\rm ion} \to 0$ for fully neutral gas.

Figure 9 shows the mass-weighted distribution of the ionization fraction as a function of the comoving gas overdensity. The contours and the gray levels are displayed on six equal logarithmic intervals in between minimum and maximum values of the projected gas mass density. The top left panel indicates that most of the gas at $t = t_0$ is fully ionized except for a pockets of neutral gas in star forming regions at $\log \rho / \langle \rho \rangle \sim 6.0$. At even higher densities ($6 < \log \rho / \langle \rho \rangle < 8$), the gas is ionized again due to supernovae feedback.

The neutral fraction in star forming regions (corresponding to the narrow contour structure extending down to the lower-right corner of each panel at $\log \rho / \langle \rho \rangle > 6$) continues to grow until $t \approx t_0 + 2t_{\rm H}$, but diminishes afterwards as the neutral gas is consumed by star formation. Additional infall onto virialized halos is suppressed in an exponentially expanding universe. After $t = t_0 + 3t_{\rm H}$, recombination is only important in the dense cores of virialized halos, and the IGM remains ionized as it continues to expand and cool. The distribution of $F_{\rm ion}$ in the IGM does not evolve at later times.

Figure 10 shows the mass-weighted distribution function of the gas mass as a function of its ionization fraction, i.e. $df_M/d\log F_{\rm ion}$. The lower end of the distribution gradually extends to lower $F_{\rm ion}$ values between $t = t_0$ and $t = t_0 + 3t_{\rm H}$, although most of the mass is still fully ionized ($\log F_{\rm ion} = 0.$). At $t = t_0 + 3t_{\rm H}$, 99% of the gas mass has an ionization fraction higher than 80%. Subsequently, the $F_{\rm ion}$ distribution freezes outside the dense cores of virialized halos.

In our simulation, we have assumed that the gas is optically thin and in ionization equilibrium when computing the abundance of different ionic species. This assumption is of course only valid in the high density region where the collisional ionization and recombination time scales are shorter than the Hubble time. We find that the ionization fraction evolve only for $\log(\rho / \langle \rho \rangle) > 4$ until $t = t_0 + 3t_{\rm H}$. In this regime of densities, the recombination rate is still higher than $1/t$, and the assumption of ionization equilibrium is justified. After $t = t_0 + 3t_{\rm H}$, the recombination time-scale becomes much longer than the Hubble time for most of the plotted range of densities, and the distribution of ionization fraction of the IGM is expected to freeze for gas that has not assembled into dark matter halos.

9 Conclusions

We have simulated the future evolution of the intergalactic medium in a universe dominated by a cosmological constant, focusing on the overdensity, temperature, and ionization fraction of the cosmic gas.

We have found that within a few Hubble times from the present epoch, the baryons will split into two major phases: one phase of low-density, low-temperature, diffuse IGM which cools adiabatically (with $T \propto a^{-2}$; see Figure 7), and a second phase of high-density, high-temperature gas in virialized dark matter halos which cools more slowly by up to two orders of magnitude [see Equation (3)]. The mass fraction of gas which is confined in virialized dark matter halos (defined as regions with an overdensity larger than ~ 200) converges to $\sim 40\%$ at late times, about twice its calculated value at the present epoch.

The simulated maps of gas temperature show that the large-scale filaments disperse and merge with the low-temperature IGM background after a few Hubble times, and only the 'island universes' of virialized gas maintain their physical structure. Although these islands are linked by filaments of dark matter and gas in comoving coordinates, the filaments rarefy and disperse in physical coordinates due to the exponential temporal growth of the cosmic scale factor, a. We do not find evidence for fragmentation of the baryons in the IGM at later times above the mass-scale of $M_{gas} \sim 5 \times 10^{11} h^{-1} M_{\odot}$.

The recombination time of the expanding IGM exceeds the Hubble time by a factor that grows rapidly in the future, and so most of the IGM gas remains ionized. After three Hubble times from the present epoch, 99% of the gas mass maintains an ionization fraction above 80%. If the Universe is indeed dominated by a true cosmological constant, then the diffuse IGM outside virialized dark matter halos will get extremely cold but remain highly ionized.

Acknowledgements

We thank Volker Springel and Lars Hernquist for helpful discussions and for allowing us to use the updated parallel version of the GADGET code which is described in Springel & Hernquist (2002, 2003a,b). This work was supported in part by the grants ATP02-0004-0093 from NASA and AST-0071019, AST-0204514 from NSF for AL. The simulations were performed at the Center for Parallel Astrophysical Computing at Harvard-Smithsonian Center for Astrophysics.

References

Adams, F. C. & Laughlin, G. 1997, Rev. Mod. Phys., 69, 337 (1997RvMP...69..337A)

Bahcall, N. A. & Bode, P. 2003, ApJ, 588, 1 (2003ApJ...588L...1B)

Becker, R. H., et al.2001, AJ, 122, 2850 (2001AJ....122.2850B)

Busha, M. T., Adams, F. C., Wechsler, R. H., Evrard, A. E., ApJ, 596, 713 (2003ApJ...596..713B)

Carroll, S. M., Press, W. H., & Turner, E. L., ARA&A, 1992, 30, 499 (1992ARA&A..30..499C)

Cen, R. & Ostriker, J. P., 1999, ApJ, 514, 1 (1999ApJ...514....1C)

Chiueh, T. & He, X-G., 2002, Phys. Rev. D, 65, 123518 (2002PhRvD..65l3518C)

Davé, R., et al., 2001, ApJ, 552, 473 (2001ApJ...552..473D)

Davé, R., Hernquist, L., Katz, N., Weinberg, D. H., 1999, ApJ, 511, 521 (1999ApJ...511..521D)

de Bernardis, P., et al., 2000 Nature, 404, 955 (2000Natur.404..955D)

Eke, V. R., Cole, S., Frenk, C. S., Patrick-Henry, J., 1998, MNRAS, 298, 1145 (1998MNRAS.298.1145E)

Eisenstein, D. J. & Hut, P. 1998, ApJ 498, 137 (1998ApJ...498..137E)

Garnavich, P. M., et al., 1998, ApJ, 509, 74 (1998ApJ...509...74G)

Gudmundsson, E. H. & Björnsson, G., 2002, ApJ, 565, 1 (2002ApJ...565....1G)

Hanany, S., et al., 2000, ApJ, 545, L5 (2000ApJ...545L...5H)

Haardt, F. & Madau, P., 1996 ApJ, 461, 20 (1996ApJ...461...20H)

Heath, D. J., 1977, MNRAS, 179, 351 (1977MNRAS.179..351H)

Hui, L. & Gnedin, N., 1997, MNRAS, 292, 27 (1997MNRAS.292...27H)

Katz, N., Weinberg, D. H., & Hernquist, L., 1996, ApJS, 105, 19 (1996ApJS..105...19K)

Krauss, L. M. & Starkman, G. D., 2000, ApJ, 531, 22 (2000ApJ...531...22K)

Loeb, A., 2002, Phys. Rev. D, 65, 047301 (2002PhRvD..65d7301L)

Nagamine, K. & Loeb, A., 2003, New Astronomy, 8, 439 (Paper I) (2003NewA....8..439N)

Nagamine, K., Springel, V., & Hernquist, L., 2003a, MNRAS, 348, 421 (2004MNRAS.348..421N)

Nagamine, K., Springel, V., & Hernquist, L., 2003b, MNRAS, 348, 435 (2004MNRAS.348..435N)

Peacock, J. A., et al., 2001, Nature, 410, 169 (2001Natur.410..169P)

Perlmutter, S., et al., 1999, ApJ, 517, 565 (1999ApJ...517..565P)

Riess, A. G., et al., 1998, AJ, 116, 1009 (1998AJ....116.1009R)

Spergel, S., et al., 2003, ApJ, 148, 175 (2003ApJS..148..175S)

Springel, V. & Hernquist, L. 2002, MNRAS, 333, 649 (2002MNRAS.333..649S)

Springel, V. & Hernquist, L. 2003, MNRAS, 339, 289 (2003MNRAS.339..289S)

Springel, V. & Hernquist, L. 2003, MNRAS, 339, 312 (2003MNRAS.339..312S)

Springel, V., Yoshida, N., & White, S. D. M., 2001, New Astronomy, 6, 79

(2001NewA....6...79S)
Verde, L., et al., 2002, MNRAS, 335, 432 (2002MNRAS.335..432V)

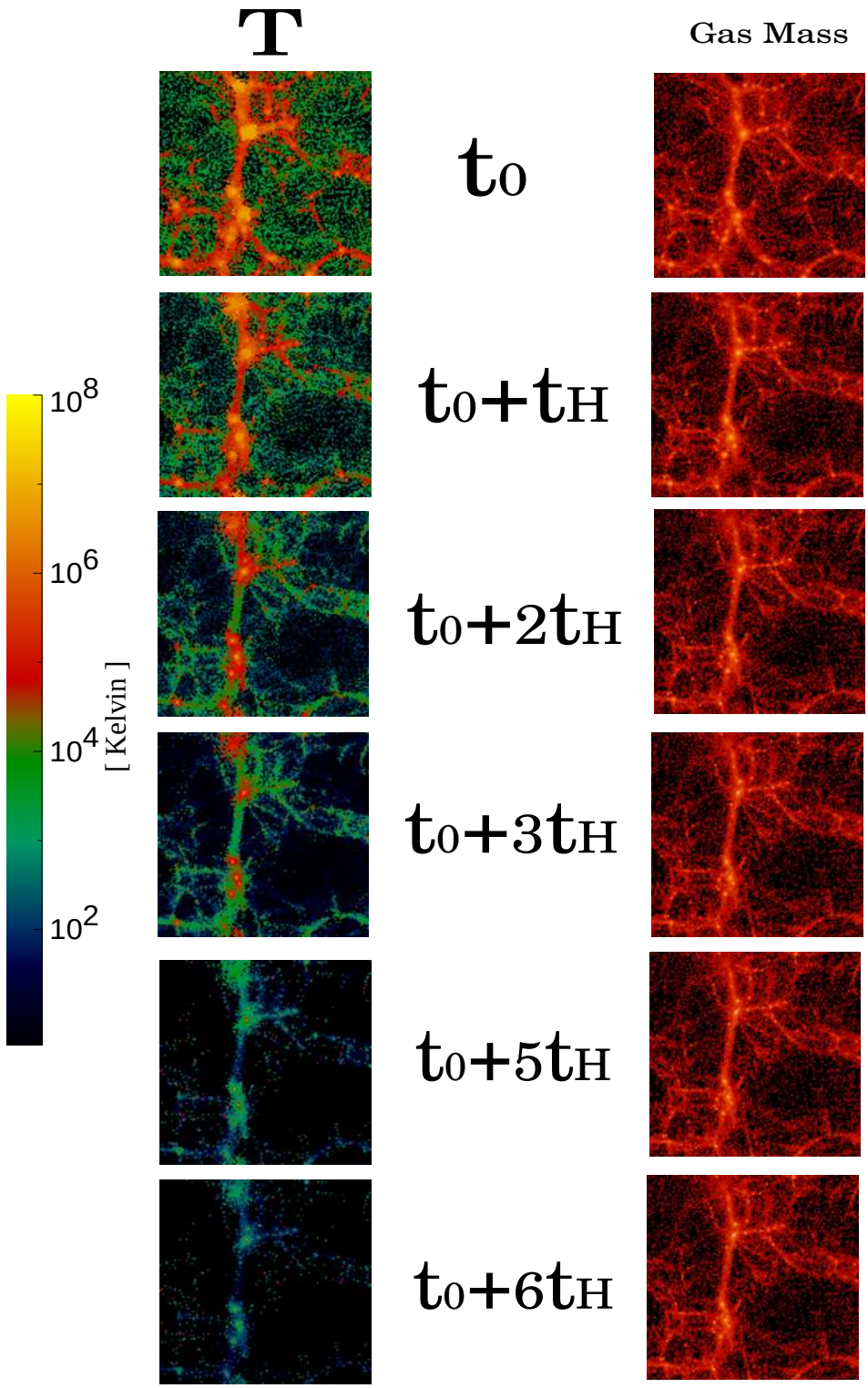

Fig. 1. Projected distribution of mass-weighted gas temperature, T, in K (left column) and projected surface gas mass density (right column) for a slice with a comoving thickness of $10h^{-1}$ Mpc and a comoving width of $50h^{-1}$ Mpc on a side.

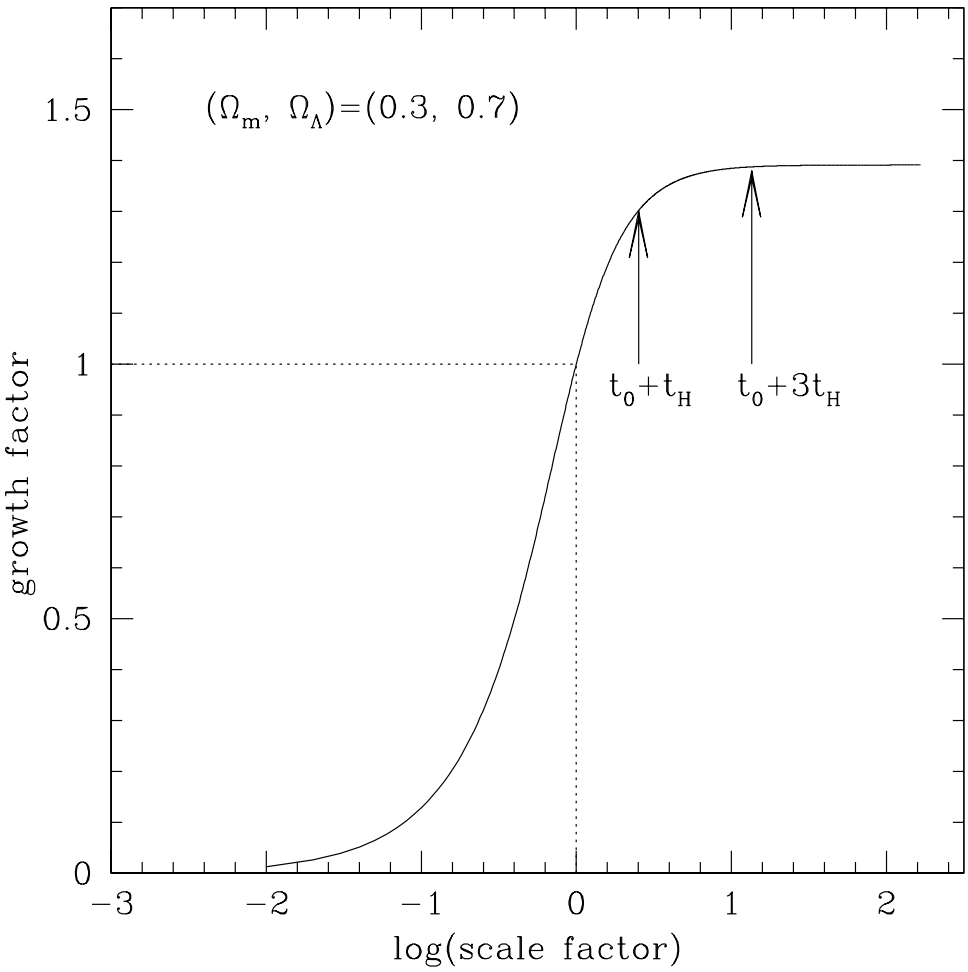

Fig. 2. Growth factor as a function of the scale factor 'a'. The curve is normalized to unity at $a = 1$, as indicated by the dotted line. The growth factor saturates within two Hubble times from the present epoch.

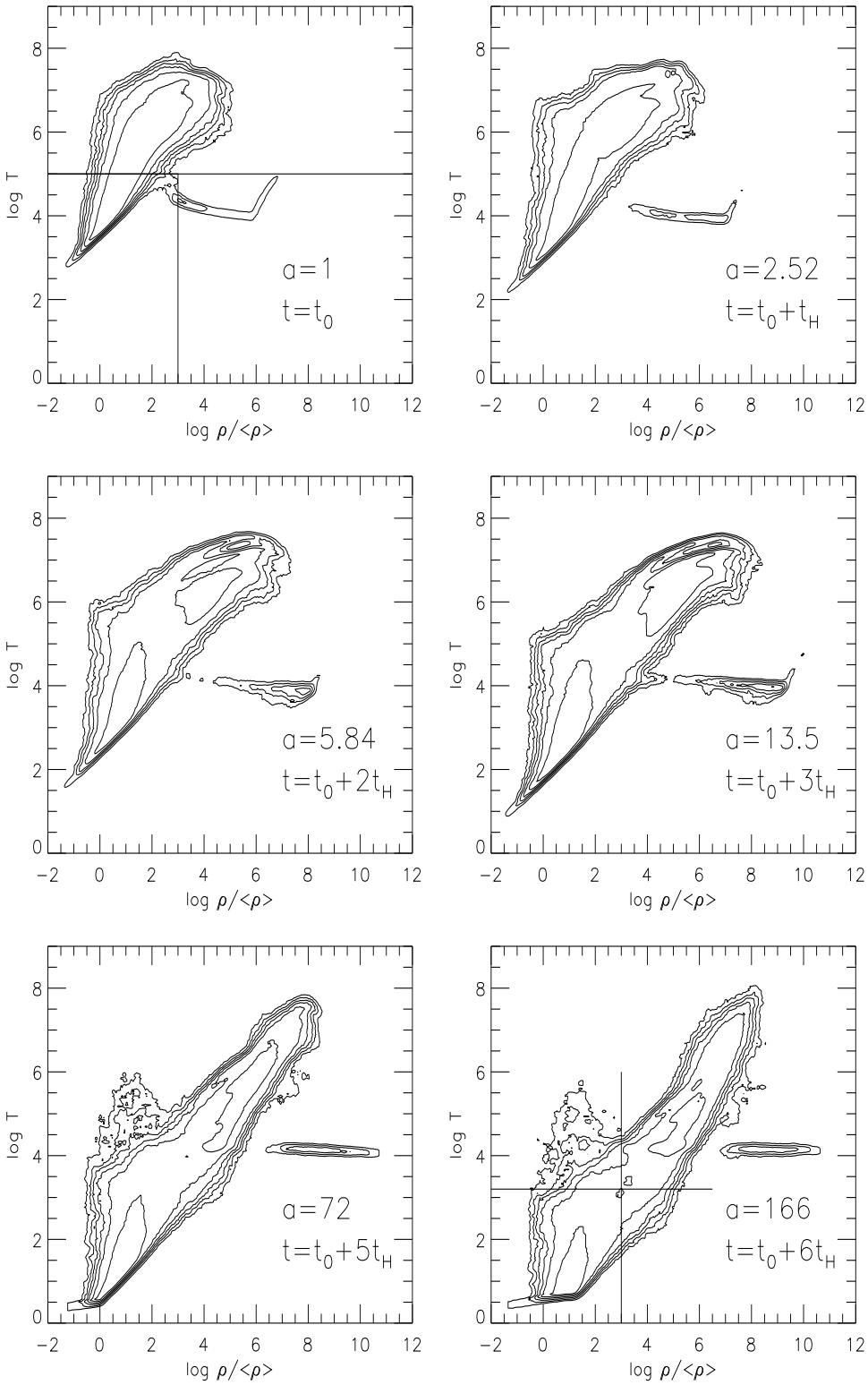

Fig. 3. Snapshots of the mass-weighted gas temperature T (in K) vs. gas density (relative to the mean value $\langle\rho\rangle$ at each epoch) for $t = t_0$, $t_0 + t_{\rm H}$, $t_0 + 2t_{\rm H}$, $t_0 + 3t_{\rm H}$, $t_0 + 5t_{\rm H}$, and $t_0 + 6t_{\rm H}$. The six contours are equally spaced in logarithmic intervals between the minimum and maximum values of the gas mass distribution on the plane. See the text for the description of the solid lines in the top left and bottom right panels.

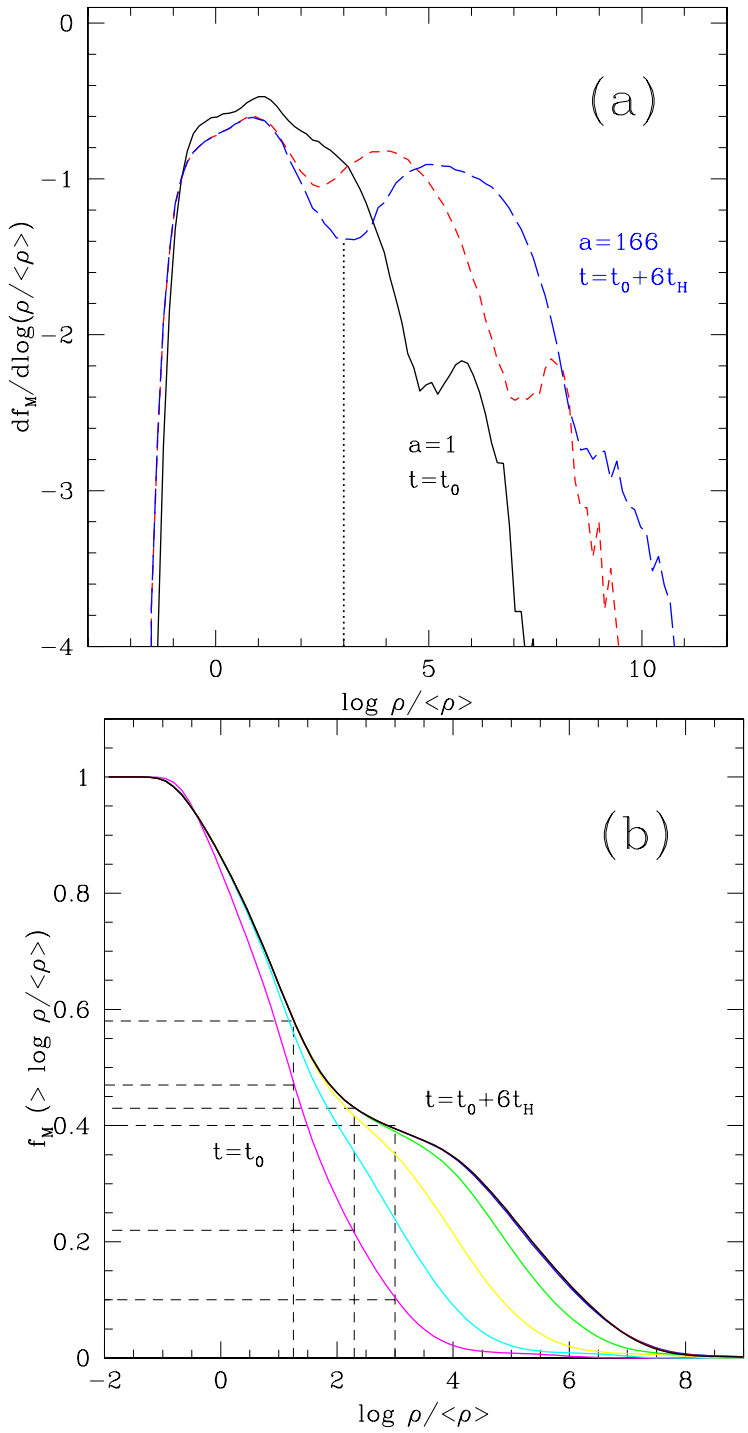

Fig. 4. *Panel (a):* Mass-weighted, differential distribution function of gas overdensity (relative to the mean density $\langle\rho\rangle$ at each epoch), i.e. $df_M/d\log(\rho/\langle\rho\rangle)$, for $t = t_0$, $t_0 + 2t_{\rm H}$, and $t_0 + 6t_{\rm H}$ from left to right. Hereafter we denote the gas mass fraction in general by f_M. A density contrast of 10^3 is indicated by the dotted line which splits the distribution into two regimes at $t = t_0 + 6t_{\rm H}$. *Panel (b):* Cumulative gas mass fraction with overdensity above a specific value, i.e. $f_M(> \rho/\langle\rho\rangle)$, for $t = t_0$, $t_0+2t_{\rm H}$, $t_0+3t_{\rm H}$, $t_0+4t_{\rm H}$, $t_0+5t_{\rm H}$ and $t_0+6t_{\rm H}$, from left to right. The characteristic values to note are indicated by the dashed lines, and are described in the text.

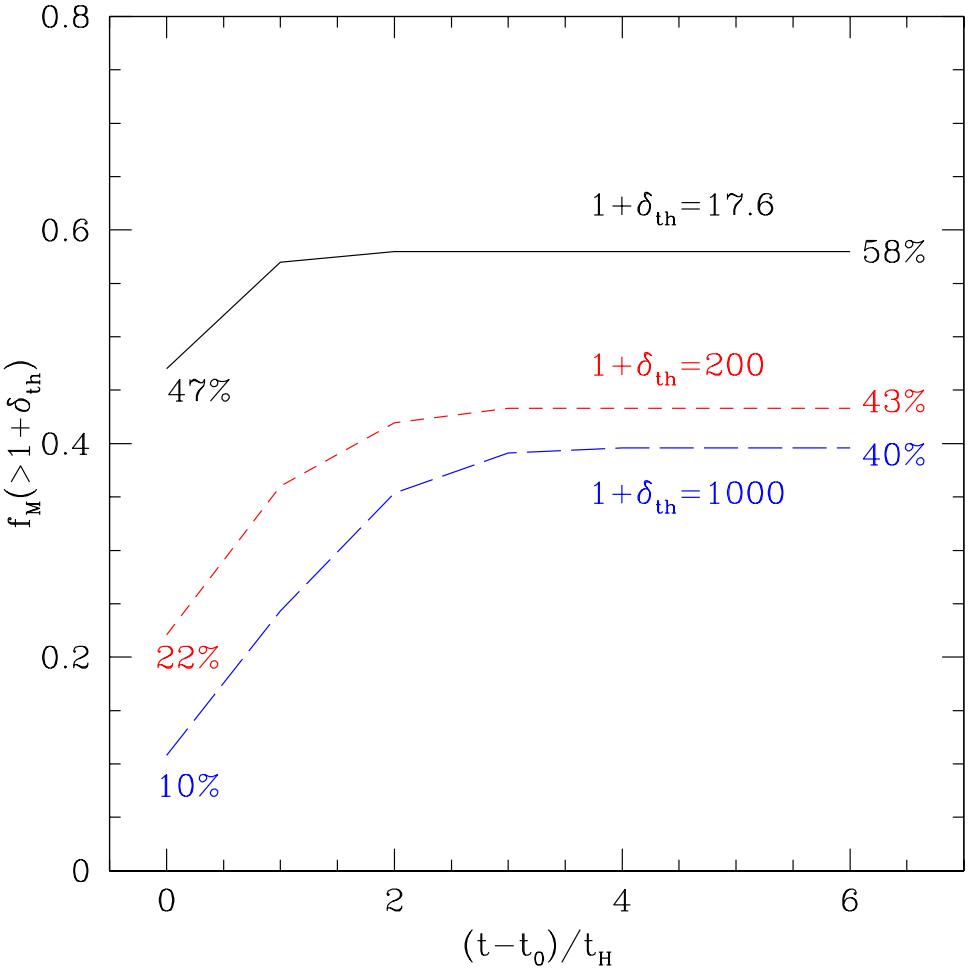

Fig. 5. Gas mass fraction $f_M(> 1 + \delta_{\rm th})$ with density contrast higher than $1 + \delta_{th} = \rho/\langle\rho\rangle = 17.6$ (solid), 200 (short-dashed), and 1000 (long-dashed line), as a function of cosmic time from the present epoch in units of the current Hubble time. The initial and final values of the gas mass fractions over the plotted range of time are mentioned next to each of the curves.

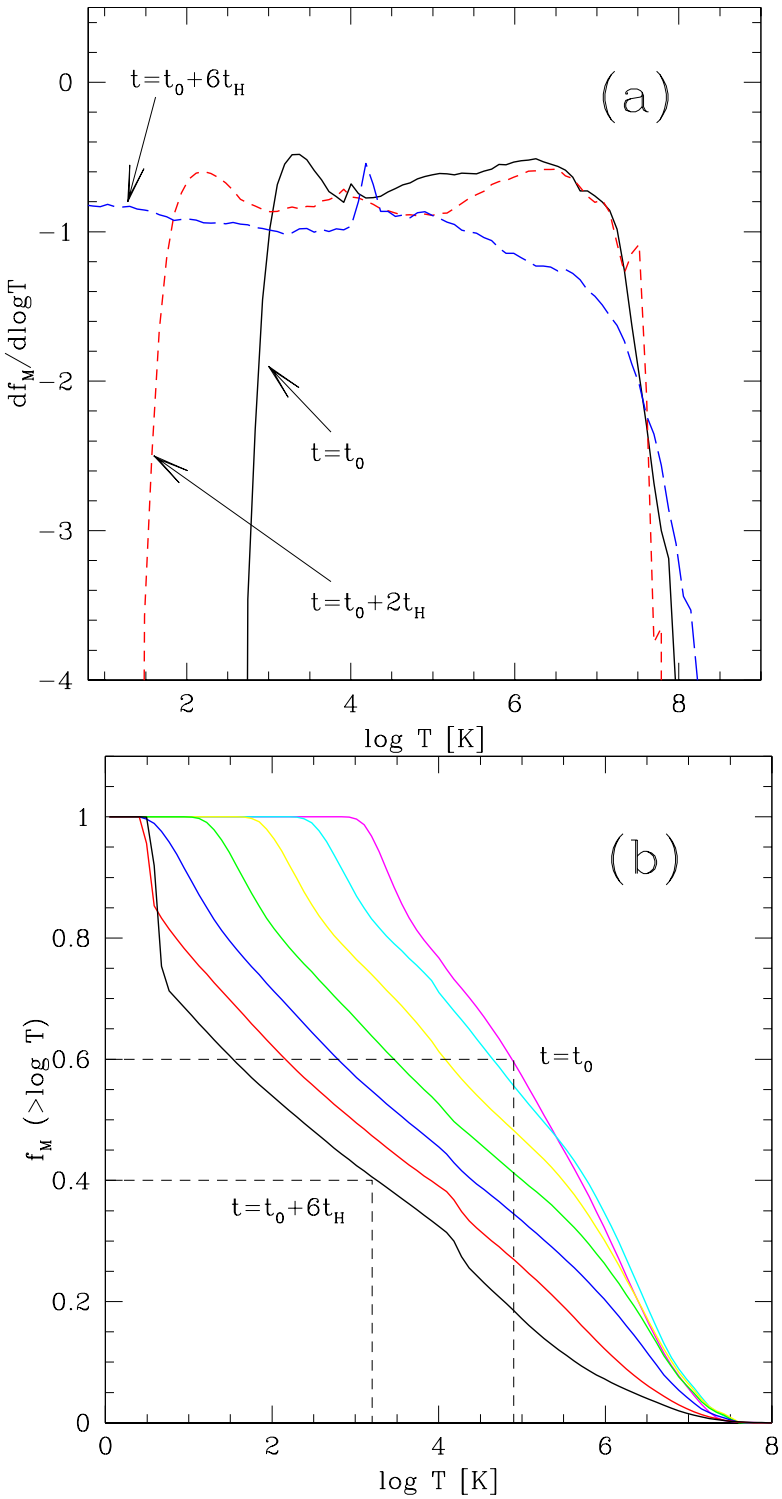

Fig. 6. *Panel (a):* Mass-weighted, differential distribution function of gas temperature T (in K), i.e. $df_M/d\log T$, at $t = t_0$, $t_0 + 2t_{\rm H}$, and $t_0 + 6t_{\rm H}$. The distribution is truncated artificially at $\log(T/{\rm K}) = 0.7$. *Panel (b):* Cumulative mass fraction of gas with temperature above a certain value for $t = t_0$, $t_0 + 2t_{\rm H}$, $t_0 + 3t_{\rm H}$, $t_0 + 4t_{\rm H}$, $t_0 + 5t_{\rm H}$, and $t_0 + 6t_{\rm H}$ from right to left. See the text for the description of the dashed lines.

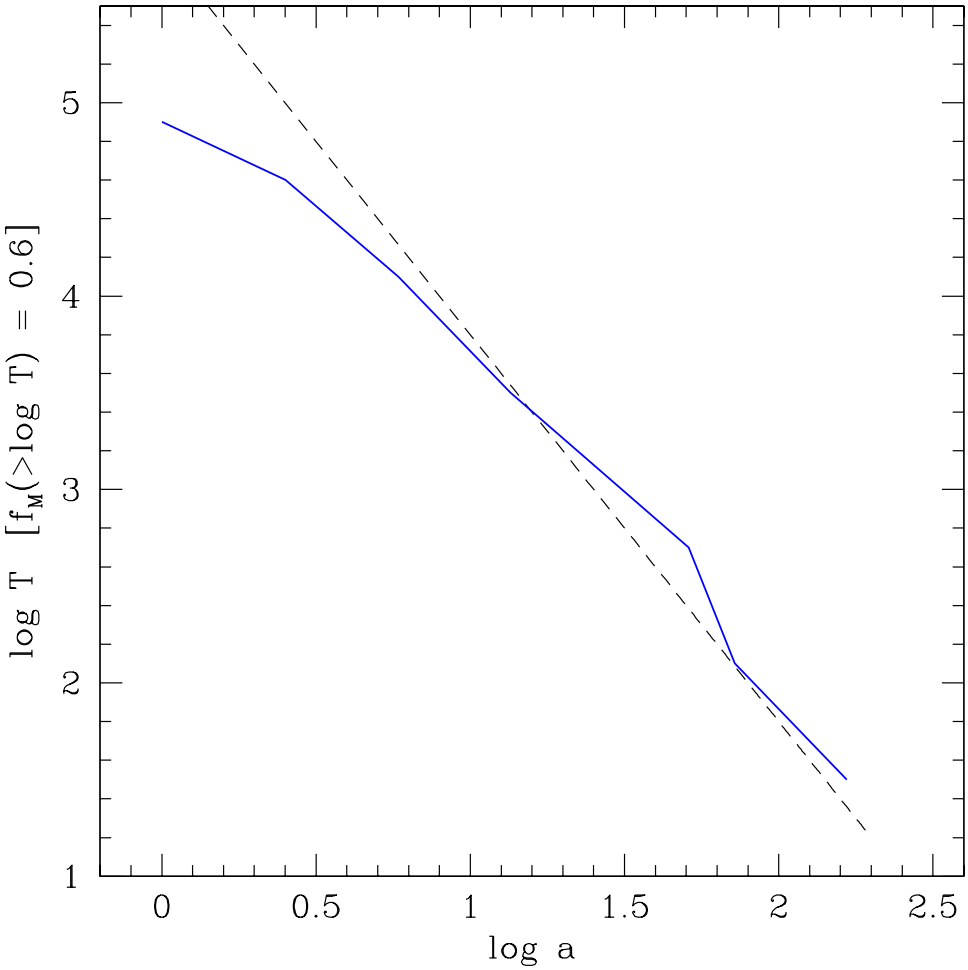

Fig. 7. Evolution of the maximum temperature for gas with a fixed mass fraction of 40% in lower density regions as a function of the logarithm of the scale factor. This quantity measures the evolution of the temperature at the fixed value of $f_M(> \log T) = 0.6$ in panel (b) of Figure 6 because Figure 6 is a cumulative plot. The curve indicates that the temperature of the diffuse IGM cools roughly according to the adiabatic expansion law $T \propto a^{-2}$, shown by the dashed line.

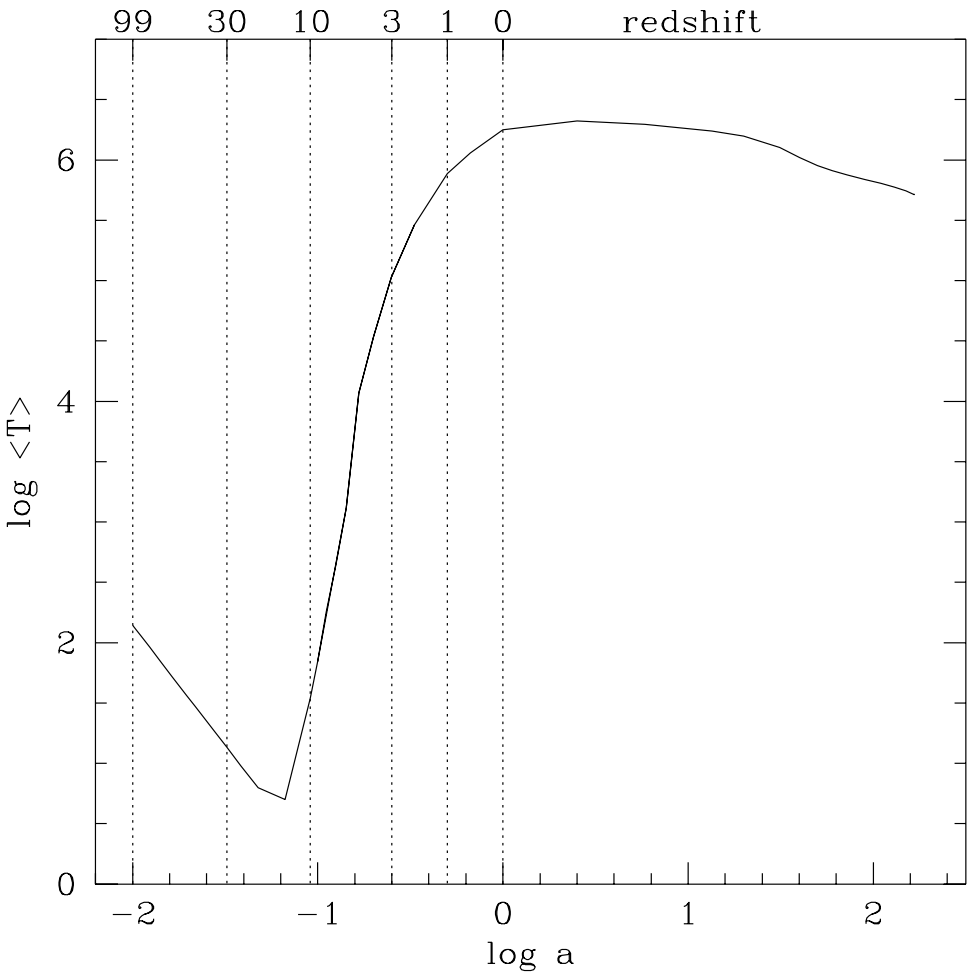

Fig. 8. Mass-weighted mean temperature of the gas in the Universe, $\langle T \rangle$, as a function of the scale factor, $a = (1+z)^{-1}$. The upper horizontal axis indicates the corresponding redshift, z.

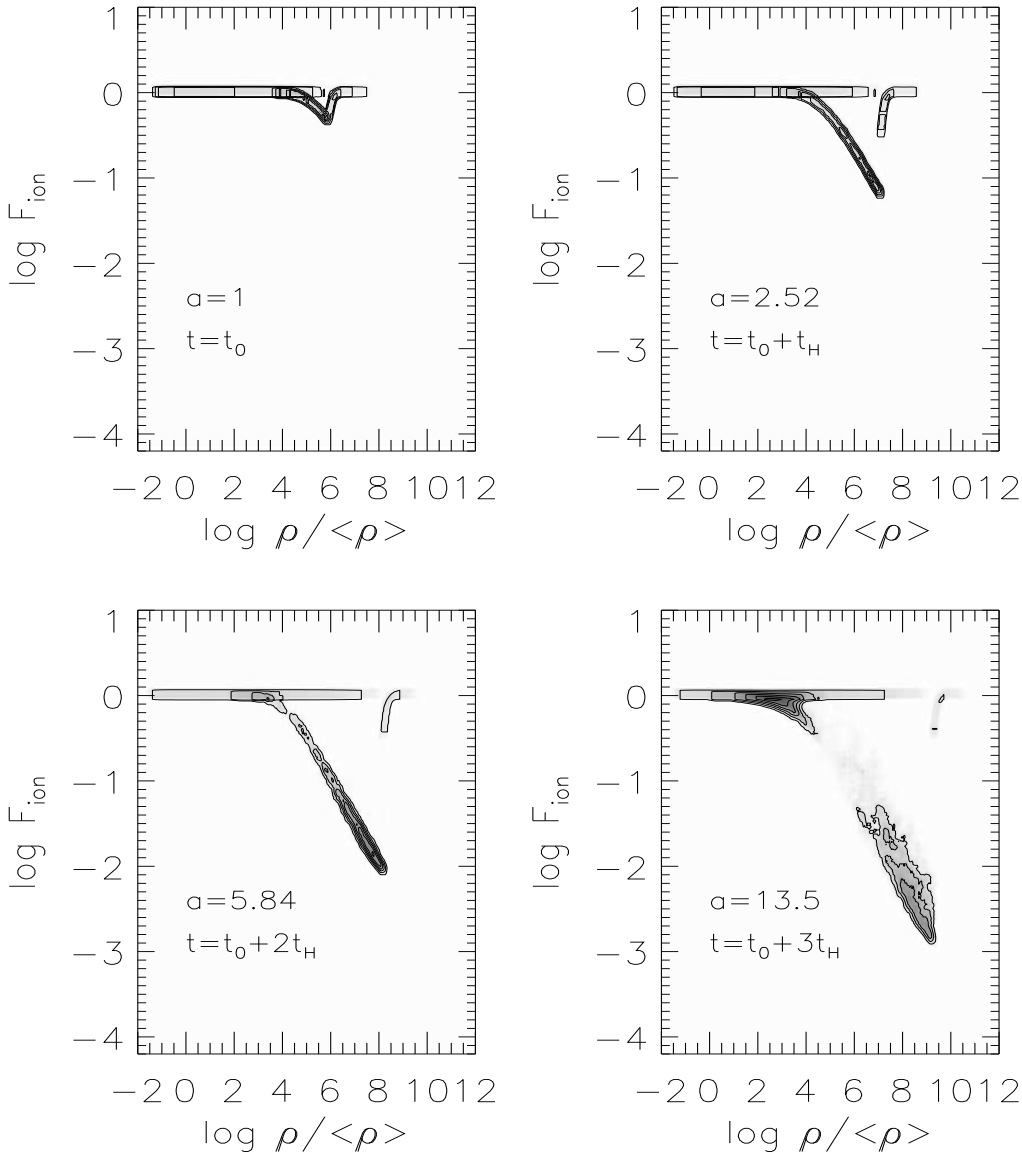

Fig. 9. Mass-weighted distribution of ionization fraction of gas as a function of gas overdensity (relative to the mean value $\langle\rho\rangle$) at $t = t_0$, $t_0 + t_{\rm H}$, $t_0 + 2t_{\rm H}$, and $t_0 + 3t_{\rm H}$. The six contour levels are equally spaced in logarithmic intervals between the minimum and maximum values of the gas mass distribution on the plane.

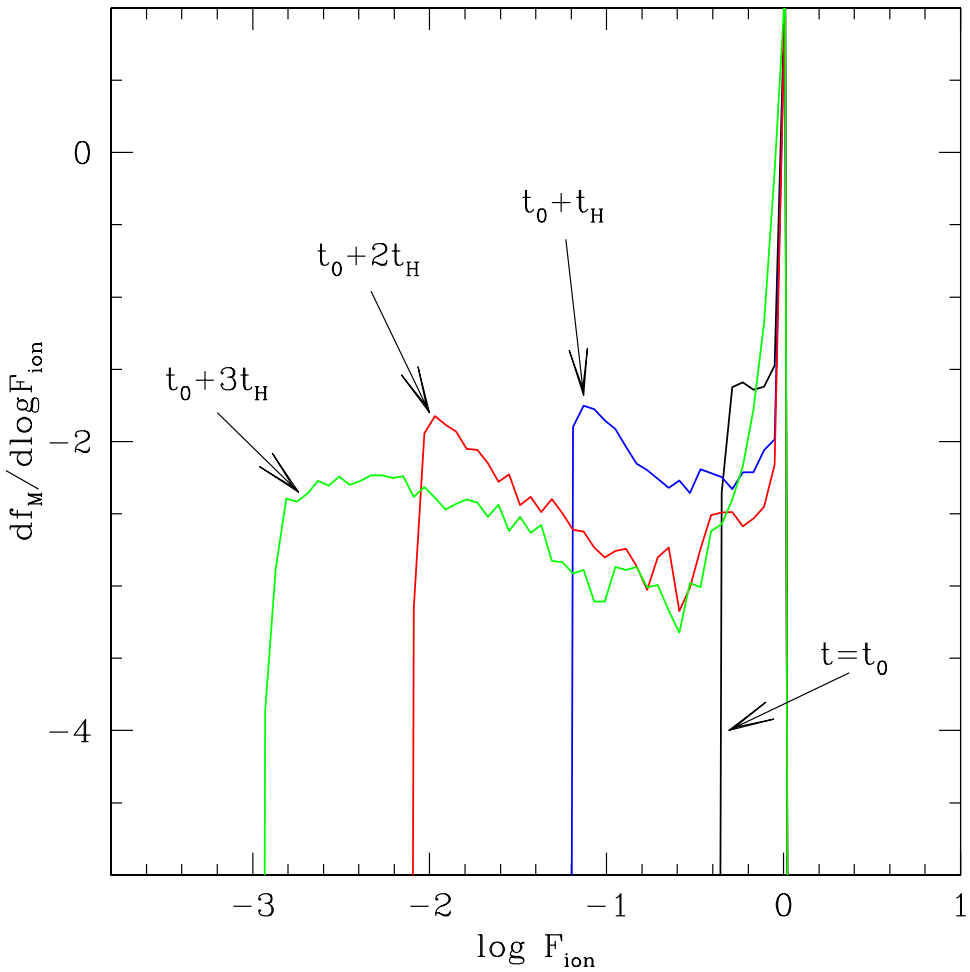

Fig. 10. Mass-weighted differential distribution function of the ionization fraction of the gas, i.e. $df_M/d\log F_{\rm ion}$, at $t = t_0$, $t_0 + t_{\rm H}$, $t_0 + 2t_{\rm H}$, and $t_0 + 3t_{\rm H}$.